

Subterranean origin of surface ripple patterns using ion beam irradiation: an extended hydrodynamical approach

Tanuj Kumar,¹ D. C. Agarwal,¹ N. P. Lalla,² and D. Kanjilal¹

¹Inter-University Accelerator Centre, Aruna Asaf Ali Marg, New Delhi-110067, India

²UGC-DAE Consortium for Scientific Research, University Campus, Khandwa Road,

Indore-452017, India

Abstract

We show that the ion beam induced incompressible amorphous solid flow in terms of advection mass transport mechanism leads to the erosion and deposition of atoms at the amorphous/crystalline (a/c) interface resulting in the formation of pattern at the a/c interface as well as at the free surface. The ion beam impact generated erosion and mass redistribution at the free surface [proposed by Bradley-Harper (BH) and its extended theories] are found to be irrelevant in patterning of surface. By varying the location of a/c interface, it has been established that a/c interface plays the prominent role in surface patterning. The morphological variation of Si surface after 50 keV Ar⁺ ion bombardment has been investigated by atomic force microscopy (AFM) and cross-sectional transmission electron microscopy (X-TEM) as a function of ion fluence. We propose a new approach that Navier-Stokes flow inside the amorphous layer coupled with the Exner equation successfully explains the growth mechanism of surface patterning.

Introduction

Ion beam sputtering has proven to be a very elegant and cost-effective single step approach for the generation of well controlled nanostructures of different topographies by varying the ion beam parameters *viz.* energy, fluence and angle of irradiation [1-2]. However, the mechanism of ion bombardment induced surface instabilities is a subject of big debate. The first theoretical approach to study the surface patterning was established by Bradley and Harper (BH) [3] on the basis of two competing processes: first one is the curvature dependent roughening which is proportional to the total energy deposited at each position on the surface as prescribed by the Sigmund theory of sputtering [4], and second one is the surface smoothing either by thermal diffusion or by ion enhanced diffusion. Indeed, BH's linear theory explained many experimentally observed ion beam sputtering (IBS) induced nano-patterning e.g. orientation of ripples with ion beam direction. However, it could not explain properly the kinetic roughening of surface, saturation of ripples amplitude, coarsening, and the large discrepancy in the experimentally observed and theoretically expected values of wavelength [5]. In order to overcome these limitations, refinements of BH's theory have been proposed [6] to underline the other effects during surface patterning.

Kalyanasundaram *et al.* [7] reported that the Ar irradiation of Si surface revealed that atoms in the bombarded region are not simply sputtered away, but major part of them are either displaced or redeposited around the region of origin, resulting in the formation of large craters at the point of impact. Several researchers have studied an impact induced mass redistribution effect in terms of molecular dynamics (MD) as an improvement over BH model [8-9]. Castro *et al.* [10] proposed the generalized framework of hydrodynamic approach, which seems to be more fundamental in identifying the underlying physical processes involved in the surface patterning by ion beam sputtering based on general conservation laws of mass and momentum. It was generally believed that the ion induces the sputtering and mass redistribution on the surface result in patterning of the surface. In that case the growth formation of ripples would have been independent of the depth location of amorphous to crystalline (a/c) interface. The aim of this research work is to establish the fact that the a/c interface plays the prominent role in formation of ripple pattern on the surface.

Experimental

In order to study the role of a/c interface in surface patterning of Si (100) surface during irradiation using energetic ion, the depth location of a/c interface is varied. The depth location of a/c interface variation is achieved by irradiating the Si surface using 50 keV Ar⁺ ion at a fluence of 5×10^{16} ions/cm² at different angles of incidence viz. 60° and 0° with respect to surface normal. These two sets of samples having different depth location of a/c interface are named as set-A (60°) and set-B (0°) respectively. The depth location of a/c interface would be higher in set-B samples as compared to set-A samples due to higher projected ion range for 0° (set-B) as compared to 60° (set-A) ion beam irradiation. After that both set samples were irradiated at room temperature for the fluences of 3×10^{17} ions/cm² to 9×10^{17} ions/cm² at an angle of 60° with respect to surface normal using 50keV Ar⁺ ion beam. The schematic view of our motivation behind the experiment work is presented in Fig 1. From Fig. 1, one can see that for further ion beam irradiation the ion beam effect is directly arriving at the a/c interface for the set-A samples while it remains inside the amorphous layer for set B samples due to deeper depth location of a/c interface. During the irradiation the base pressure of chamber was maintained at $\sim 10^{-7}$ mbar. The ion beam current density was kept constant at $15 \mu\text{A}/\text{cm}^2$. The beam was scanned uniformly over an area of 10 mm×10 mm by electrostatic scanner. After irradiation, the samples were analyzed by Nano Scope IIIa atomic force microscope (AFM) under ambient conditions in tapping mode. Cross-sectional transmission electron microscopy (XTEM) was carried using a Tecnai-G2-20 TEM facility operating at 200 kV. The cross-sectional specimens for TEM study were prepared by using Ar ion-beam milling at 4 kV/20 μA and at an angle of incidence of 4° with respect to the sample surface.

Results and discussion

Fig. 2(a) and (b) show the AFM images of Si surface irradiated at the fluence of 5×10^{16} ions/cm² at two different angles of 60° and 0° with respect to surface normal. These two sets of samples are named as Set-A and Set-B respectively. It is found that the microstructure of the surface is same in both sets of the samples having nearly similar average rms roughness values of 0.5 ± 0.1 nm and 0.6 ± 0.1 nm respectively. AFM images of further ion beam irradiated samples

(set-A and set-B) at the fluences of 3×10^{17} ions/cm², 5×10^{17} ions/cm², 7×10^{17} ions/cm² and 9×10^{17} ions/cm² are shown in Fig. 3. From Fig. 3(a-d), it is found that for the set-A, the increase in ion fluence leads to formation of ripples, which are oriented perpendicular to ion beam direction. However, in set-B samples, minor signature of formation of ripples with much smaller amplitude is observed under same irradiation condition. For set-A (Fig. 4(a)), the observed amplitude of ripples follows exponential growth as $h \propto \exp(\phi/\phi_o)$, where ϕ_o is a fitting parameter. Using this relation, the experimental data has been fitted for amplitude, which predicts that $\phi_o = 2.3 \times 10^{17}$. This exponential growth of amplitude is in accordance with existing linear BH theory. However, for set-B the observed average amplitudes of ripples are about one order of lower in magnitude compared to those for set-A samples at corresponding fluences. Fig. 4(b) shows that the magnitudes of wavelengths of ripples are similar for both sets of samples at corresponding irradiated fluences. The wavelength of ripples varies linearly at a rate of 30.7 ± 1.4 nm/ 10^{17} ions cm⁻² and 28 ± 0.6 nm/ 10^{17} ions cm⁻² for set-A and set-B samples respectively. As per the predictions of BH model [3] wavelength of ripples should be independent of fluence. Despite of similar initial surface morphology of both sets of samples (Fig.2), the observed similar wavelength of ripples and negligible ripple amplitude in set-B samples as compared to set-A samples after irradiation cast doubt on the validity of Bradley-Harper and its extended theories which are based on curvature dependent sputtering and surface diffusion. The prominent role of the a/c interface in formation of ripples is established in this work.

Fig. 5 shows the cross-sectional TEM images taken from the sample irradiated at 0° with a fluence of 5×10^{16} ions/cm², and samples of set-A irradiated at fluences of 3×10^{17} ions/cm², 7×10^{17} ions/cm² and 9×10^{17} ions/cm² respectively. Fig. 5(a) shows that the top amorphous layer has a uniform thickness of about 170 nm. From Fig. 5(b), one can see that the ion irradiation at the fluence of 3×10^{17} ions/cm² produces a top amorphous layer having the uniform thickness of around 75 nm. The estimated amorphous layer thickness is non-uniform having front slope (side facing the ion beam) thickness of 85 nm, which is slightly thicker than rear slope (opposite direction) thickness of 64 nm at the fluence of 5×10^{17} ions/cm² which is similar to that observed by Chini *et al.* [11]. In a similar fashion, for the fluence of 7×10^{17} ions/cm², the measured front slope thickness is 110nm and rear slope thickness is 55 nm. It clearly reveals that thickness of front edge increases and thickness of rear slope decreases on increasing the ion fluence. From the XTEM images and using grid line method, it is found that during the rippling processes the

overall cross-sectional area of amorphous layer remains constant. The formation of rippled structure at interface clearly demonstrates the role of a/c interface in the process of formation of ripples.

In order to explain the ripples formation mechanism by ion beam irradiation, we divide the discussion in to two parts:

- (1) Mass redistribution
- (2) Hydrodynamic model

(1) Mass redistribution:

In linear regime of Bradley-Harper (BH) theory, the ripples formation of a flat and isotropic surface arises due to curvature dependent sputtering mechanism and various smoothing processes [3]. The surface evolution with sputtering time is given by

$$\frac{\partial h(x, y, t)}{\partial t} = S_x(\theta)\partial_x^2 h + S_y(\theta)\partial_y^2 h - D\nabla^4 h + \eta(x, y, t) \quad (1)$$

where $S_x(\theta)$, $S_y(\theta)$ correspond to curvature dependent coefficients related to surface instability when negative, and vice versa. The coefficient D corresponds to the ion induced surface diffusion. $\eta(x, y, t)$ is white noise with zero mean resulting from stochastic nature of ion arrival to the surface. Using the Fourier transformation of equation 1, the surface amplification rate $R(q)$ is given by

$$R(q) \equiv \text{Re}(\omega(q)) = -S_x q_x^2 + S_y q_y^2 - D(q_x^2 + q_y^2)^2 \quad (2)$$

The stability or instability of a surface is a function of the sign of the maximum growth rate $\max\{R(q)\}$. For the formation of ripples in the direction parallel to the ion beam direction (x-direction), S_x is the dominant parameter over S_y . Also, the curvature co-efficient $S_x(\theta)$ can be decomposed in to two components, namely, ion-stimulated erosive component $S_x^{eros}(\theta)$ and redistributive component $S_x^{redist}(\theta)$, which can be evaluated using the BH erosive model [3] and Carter- Vishnyakov ion induced mass redistribution model [12] respectively. Madi *et al.* [13] has reported the modification of $S_x(\theta)$ using Yamakura correction factor. With this modification, $S_x(\theta)$ can be calculated by following equations [13,14].

$$S_{x,y}^{eros.}(\theta) = Ja\Omega\Gamma_{x,y}(\theta)Y(\theta) \quad (3)$$

$$S_x^{redist.}(\theta) = J\delta\Omega\cos(2\theta)\exp\left[\frac{-\Sigma}{\cos(\theta)}\right] \quad (4)$$

where J is the ion flux, a is the ion range, Ω is the Si atomic volume, $Y(\theta)$ is the sputtering yield of the flat surface, $\Gamma_{x,y}$ represent the coefficients of curvature, and δ is the net recoil displacement.

Using the same formulation, the value of erosive term $S_x^{eros}(\theta)$ and redistributive term $S_x^{redist}(\theta)$ have been calculated using $J = 1 \times 10^{14}$ ions/cm²s, $a = 56$ nm, $\Omega = 2 \times 10^{23}$ cm³ for our experimental results. The values of net recoil displacement (δ) are 10 nm for 250 eV Ar ion [9] and 65 nm for 1000 eV Ar ion [13] respectively. Based on these reported works, the recoil displacement is estimated to be 3000 nm for 50 keV Ar ion. The calculated values of $S_x^{eros}(\theta)$ and $S_x^{redist}(\theta)$ are -2.04×10^{-3} nm²/s and -81.27×10^{-3} nm²/s respectively. The smaller magnitude of $S_x^{eros}(\theta)$ as compared to $S_x^{redist}(\theta)$ suggest that the sputter erosion is essentially irrelevant in surface patterning, as predicted by Madi *et al.* [13] and Norris et al [9]. Despite of similar initial surface morphology the prominent formation of ripples for set-A samples as compared to set-B samples suggest that the curvature dependent erosive terms would have minor contributions in surface patterning, but, a large mass redistribution plays crucial a role. Now a question raises here that how and where the mass redistribution solely results in the surface patterning.

(2) Hydrodynamic model

The hydrodynamic model suggested by Castro *et al.* [10] for surface rippling by ion beam sputtering (IBS) is based on the assumption that the external amorphous layer during irradiation has stationary density as well as thickness, which can be described as a highly viscous fluid. This viscous flow is similar to that proposed by P.F.A. Alkemade [15] to explain the propulsion of ripples on glass under Navier stokes flow induced by ion bombardment. With the assumption of incompressible amorphous layer flow, the fluid mechanics can be described with $\nabla \cdot \mathbf{V} = 0$, where $\mathbf{V} = ui + wk$ is the velocity field. Castro *et al.* [10] predicted the dispersion relation for ripples above the critical angle of $\theta > 45^\circ$ as

$$\omega_q' = -\frac{(q^2\sigma + f_E\partial_\theta(\sin(\theta)\Psi(\theta)))(-2dq + \sinh(2dq))}{2q\mu(1 + 2d^2q^2 + \cosh(2dq))} + \omega_q' \quad (5)$$

For the pattern generation, ω_q' in Eq. 5 should have a positive maximum for $q = q_c$, and have a characteristic wavelength given by

$$\lambda_c = \frac{2\pi}{q_c} = \frac{2\pi}{\sqrt{\left(\frac{-\sigma + \sqrt{\sigma^2 - 2d^2\sigma Z}}{2d^2\sigma}\right)}} \quad (6)$$

where $Z = f_E\partial_\theta(\sin(\theta)\Psi(\theta))$, $\Psi(\theta) = \cos\theta$, σ is the surface tension and $f_E = \text{stress/depth}$ is the body force term which contains the information about stress. Using this formulism and experimental observed parameters, the calculated value of f_E is $7.5 \times 10^{-3} \text{ kg nm}^{-2} \text{ s}^{-2}$ for an amorphous layer of 170 nm in width. Surface tension has been chosen as 1.34 J/m^2 for calculation [16]. The calculated value of wavelength is $\sim 450 \text{ nm}$. However, the more accurate measurement of stress would provide an improved estimation of calculated wavelength. The value of wavelength from this hydrodynamic theory is close to our experimental results, but this theory could not predict the mechanism of ripples formation. Based on our experimental results and theoretical calculations, we propose an extension of hydro-dynamical approach of surface rippling in terms of Exner equation. Here, we also propose that the Navier Stokes flow induced mass redistribution solely results in the formation of ripples at the a/c interface as well as at the free surface as discussed below:

Exner equation

In natural environments, sand ripples of various kinds such that Aeolian ripples (driven by the wind) and current ripples (unidirectional water flow) have been observed. Charru *et al.* [17] proposed that Navier-Stokes steady flow of water over sand bed results in the surface instability based on the erosion of grain particles by fluid flow and deposition of particles under the effect of gravity of earth on sediment bed as advection process in terms of mass conservation equation (Exner equation 1925) as

$$C \frac{\partial h}{\partial t} = -\frac{\pi d^3}{6} \frac{\partial q}{\partial x} \quad (7)$$

where C is the bed compactness, d is the grain diameter and the divergence of the flux $(\frac{\partial q}{\partial x})$ represent the net erosion rate. The slow time evolution (Eq.7) of the bed surface leads to the equation

$$h = h_0 e^{\delta t} \cos[k(x - ct)] \quad (8)$$

where c is the wave velocity and δ is the growth rate of ripples.

Same scenario has been proposed here for the mechanism(s) of formation of ripples of semiconductors' surfaces using ion beam irradiation. For clear interpretation of mechanism(s) of surface patterning, a schematic view of irradiation for both set of samples is presented in Fig.6. Here we propose that direct and/or indirect transfer of momentum to the target atoms by ion beam irradiation induces the incompressible Navier stokes flow inside the amorphous layer for both sets of samples as shown in Fig.6 (a-b). Fig. 6(a) shows that for the set-A samples, the ion beam induced incompressible Navier stokes flow inside the amorphous layer results in large amount of erosion of Si atoms and ion beam irradiation induced stress results in the deposition of Si atoms at the a/c interface [ion beam effect directly has been reaching at the a/c interface], and resulting in $\frac{\partial q}{\partial x}$ having a non-zero finite value for equation (7). Thus the amplitude of interface follows the exponential growth with time (fluence) as $h \propto h_0 e^{\delta t}$ as also observed in Fig.4 (a). So, we conclude that the mass rearrangement at the a/c interface as conservation advection transport mechanism (Exner equation) during the incompressible stokes flow results in the formation of ripples at the a/c interface as well as at the free surface.

While for set-B samples the ion beam remains inside the amorphous layer as shown in Fig 6 (b). So, there is much smaller rate of erosion and deposition of Si atoms at the a/c interface. So right hand side of Eq. 7 should be near to zero ($\frac{\partial q}{\partial x} \sim 0$), which implies that h is nearly constant. The amplitude of ripples for set-B samples is much smaller in magnitude as compared to that for set-A samples and nearly remains constant with fluences as observed in Fig. 4(a).

Charru *et al.* [18] also proposed that the selection of wavelength during ripples formation on sand bed by fluid flow depends on the deposition length (distance travelled by a particle during one flight) of particles which is closely related to equilibrium flow of sand flux with fluid flow velocity. The experimentally observed wavelengths as well as growth rate of ripples for both sets of samples (set-A and set-B) are presented in Fig. 4 (b). The observed wavelengths of ripples have similar values for both sets of samples at all irradiated fluences. In the schematic view of Fig. 6, we presented that the further ion beam irradiation of both sets of samples has been carried out using 50keV Ar⁺ ion beam irradiation at an angle of 60⁰ with respect to surface normal. So, the momentum transferred effect by ion beam inside the amorphous layer along the surface component of ion beam would be same for both sets of samples, and which results in the same velocity of solid flow in amorphous layer for both sets of samples. The same velocity of solid flow inside the amorphous layer results in the same deposition length of Si atoms for both sets of samples, which results in the same growth as well as the wavelength of ripples for both sets of samples at irradiated fluences. So, our experimental results confirm that the wavelength of ripples is strongly dependent on the rate of stokes flow inside the amorphous layer.

Conclusion

In conclusion, we have shown that when the ion beam reaches the a/c interface (for set-A) well organized formation of ripples is observed at the free surface, while an insignificant signature of ripples is seen when the ion beam remains inside the amorphous layer (for set-B). The contribution from the ion beam induced curvature dependent sputtering and mass redistribution on the free surface proposed by BH theory are essentially insignificant in surface patterning. We propose that the incompressible Navier stokes flow inside the amorphous layer induced by ion beam leads to the erosion and deposition of atoms at the a/c interface. Coupling of Navier stokes flow with the Exner equation of mass transport explains the mechanism of surface patterning.

Acknowledgement

One of the authors (TK) is thankful to Council of Scientific and Industrial Research (CSIR), India for financial support through senior research fellowship. The help received from S. A. Khan and U. K. Rao is gratefully acknowledged here.

References

- (1) S. Facsko, T. Dekorsy, C. Koerdt, C. Trappe, H. Kurz, A. Vogt, H.L. Hartnagel, *Science* **285**, 1551(1999).
- (2) R. Gago, L. Vazquez, R. Cuerno, M. Varela, C. Ballesteros and J. M. Albella, *Appl. Phys. Lett.* **78**, 3316 (2001).
- (3) R. M. Bradley and J. M. Harper, *J. Vac. Sci. Technol. A* **6**, 2390 (1988).
- (4) P. Sigmund, *Phys. Rev.* **184**, 383 (1969).
- (5) J. Kim, D. G. Cahill and R. S. Averback, *Phys. Rev. B* **67**, 045404 (2003).
- (6) W. L. Chan, E. Chason, *J. Appl. Phys.* **101**, 121301 (2007).
- (7) N. Kalyanasundaram, M. Ghazisaeidi, J. B. Freund and H. T. Johnson, *Appl. Phys. Lett.* **92**, 131909 (2008).
- (8) H. Zhou, L. Zhou, G. Ozaydin, K. F. Ludwig and R. L. Headrick, *Phys. Rev. B* **78**, 165404 (2008).
- (9) S. A. Norris, J. Samela, L. Bukonte, M. Backman, F. Djurabekova, K. Nordlund, C. S. Madi, M. P. Brenner and M. J. Aziz, *Nat. Commun.* **2**, 276 (2011).
- (10) M. Castro, R. Cuerno, Hydrodynamic approach to surface pattern formation by ion beams. *Appl. Surf. Sci.* (2011), doi:10.1016/j.apsusc.2011.09.008
- (11) T. K. Chini, F. Okuyama, M. Tanemura, and K. Nordlund, *Phys. Rev. B* **67**, 205403 (2003).
- (12) G. Carter and V. Vishnyakov, *Phys. Rev. B* **54**, 17647 (1996).
- (13) C.S. Madi, E. Anzenberg, K. F. Ludwig, Jr. and M. J. Aziz, *Phys. Rev. Lett.* **106**, 066101 (2011).
- (14) E. Anzenberg, C.S. Madi, M.J. Aziz and K.F. Ludwig Jr., *Phys. Rev. B* **84**, 214108 (2011).
- (15) P. F. A. Alkemade, *Phys. Rev. Lett.* **96**, 107602 (2006).
- (16) S. Vauth, S. G. Mayer, *Phys. Rev. B* **75**, 224107 (2007).
- (17) F. Charru and E. J. Hinch, *J. Fluid Mech.* **550**, 111 (2006).
- (18) F. Charru, *Phys. Fluids* **18**, 121508 (2006).

Figure Captions

FIG. 1 Schematic view of 50 keV Ar^+ ion beam irradiation at an angle of 60° with respect to surface normal for set-A and set-B samples. For set-A samples the ion beam effect is directly reaching at the a/c interface while it remains inside the amorphous layer for set-B samples.

FIG. 2 AFM images of 50 keV Ar^+ irradiated substrates of Si (100) at the fluence of 5×10^{16} ions/cm² for two different angles (60° for set-A and 0° for set-B) with respect to surface normal.

FIG. 3 AFM images for the 50 keV Ar^+ irradiated set-A and set-B samples at an angle of 60° with respect to surface normal at the fluences of (a) 3×10^{17} ions/cm² (b) 5×10^{17} ions/cm² (c) 7×10^{17} ions/cm² (d) 9×10^{17} ions/cm² respectively. The arrows in the figures indicate the projection of ion beam direction on the surface.

FIG. 4 Variation of amplitude and wavelength of ripples for set-A and set-B samples with ion beam fluence. The amplitude for set-A is fitted experimentally with fitting parameter $\phi_o = 2.3 \times 10^{17}$.

FIG. 5 X-TEM images of 50 keV Ar^+ irradiated substrates of Si(100) at: (a) normal incidence for the fluence of 5×10^{16} ions/cm², and an angle of 60° with respect to surface normal at different fluence of: (b) 3×10^{17} ions/cm² (c) 7×10^{17} ions/cm² (d) 9×10^{17} ions/cm².

FIG. 6 Sketch of erosion and deposition phenomenon under Navier stokes flow for (a) set-A and (b) set-B samples. The smaller rate of erosion and deposition for set-B samples as compared to set-A samples is discernible.

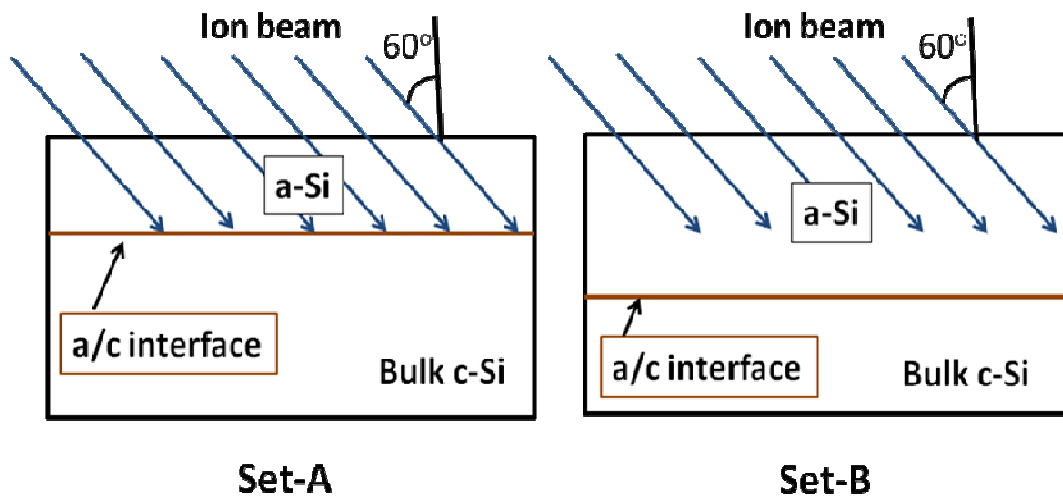


FIG. 1

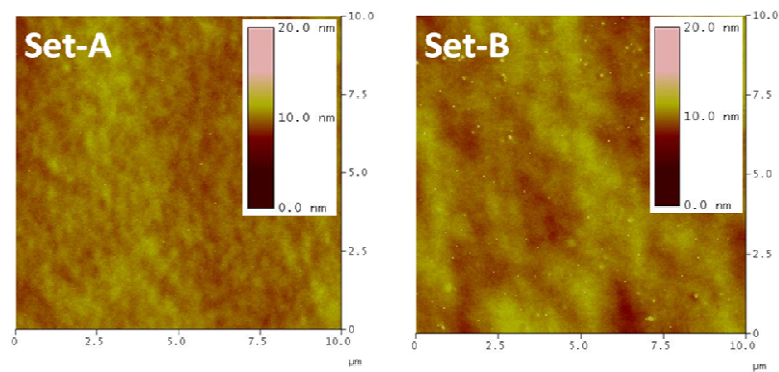


Fig. 2

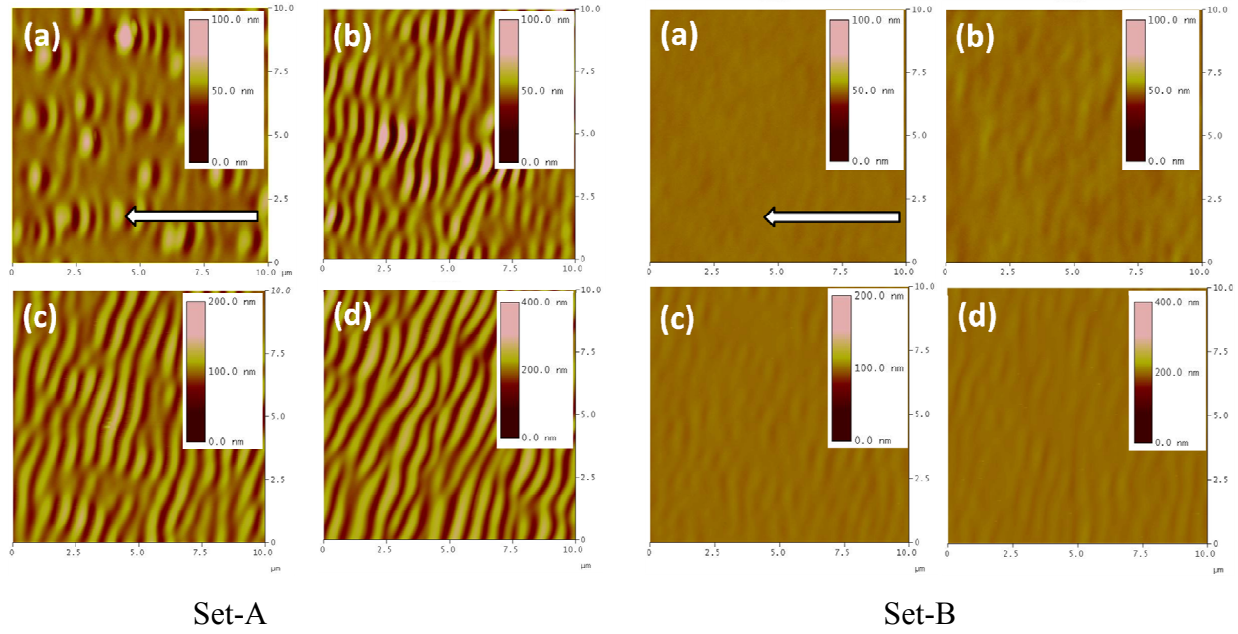


FIG. 3

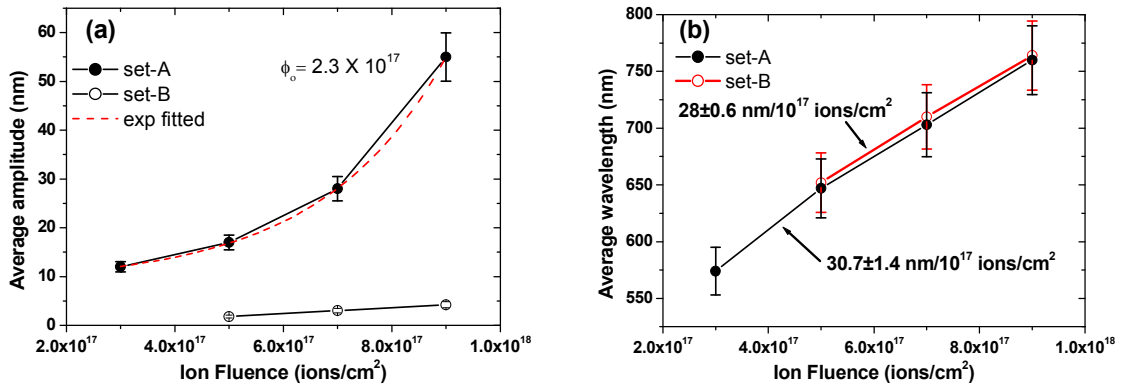


FIG. 4

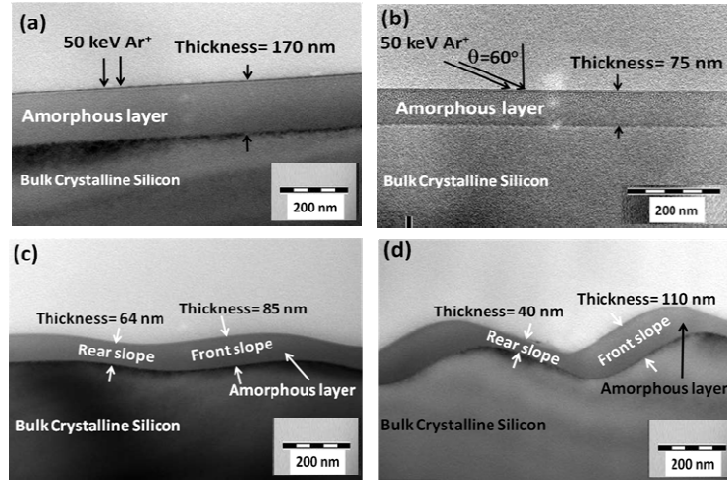


Fig. 5

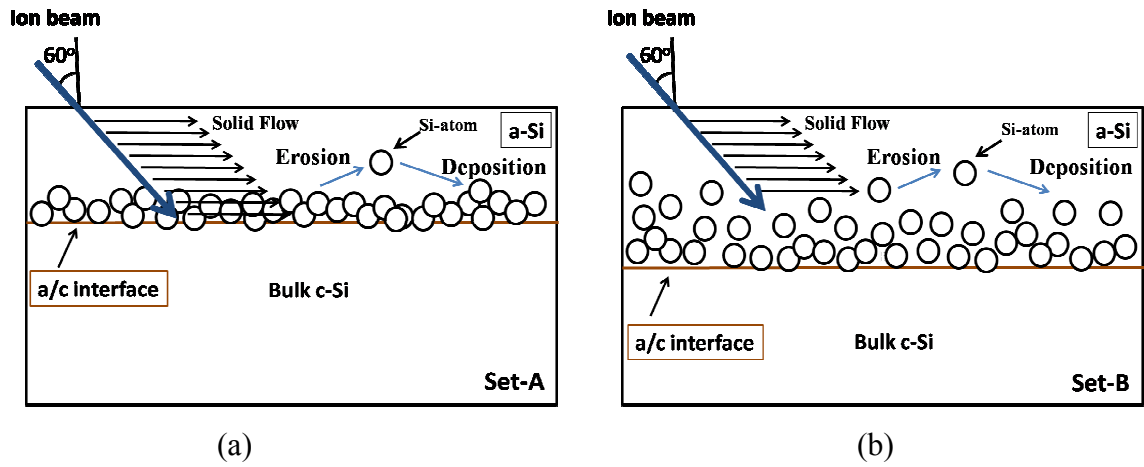


Fig. 6